

Numerical Simulation on Charge Transport in Polyethylene with Field-Dependent Parameters Under DC Electric Field

Boukhari Hamed¹, Youcef Abdallah Baadj², and Fatiha ROGTI³

¹Laboratoire Materials Energy Systems Technology and Environment, Université de Ghardaia, BP 455 Ghardaia 47000, Algérie; boukhari.hamed@univ-ghardaia.edu.dz

²Laboratoire de développement des matériaux semi-conducteur et matériaux diélectrique, Département de Génie Electrique, Université Amar Tlidji, Laghouat Route de Ghardaia BP 37, Algeria; baadjyoucef@gmail.com

³Analysis and Control of Energy Systems and Electrical Networks, University of laghouat, Algeria; f.rogti@mail.lagh-univ.dz

*Correspondence: Boukhari Hamed; boukhari.hamed@univ-ghardaia.edu.dz

ABSTRACT- During the past few years, the use of HVDC cables has increased exponentially. However, the accumulation of space charges within insulating materials remains a major challenge. Understanding the mechanisms governing this phenomenon is key to improving HVDC performance. This goal is often achieved through numerical simulations. Therefore, it is imperative that they are performed efficiently. In this work, a bipolar charge transport (BCT) model is used to offer a physical description of space charge behavior in low-density polyethylene (LDPE) under a high DC electric field. This model includes injection, migration, trapping, detrapping and recombination charges with parameters dependent on the electric field such as mobility, trapping, and recombination. The principal simulation results are dedicated to temporal and local distributions of the net charge density, electric field distribution, trapping distribution, quantity of charge mobile and trapped and evolution of external current density. The result shows that the trapping charge probability depending of the electric field in LDPE has a significant impact on the charge transport behavior compared to other properties. The trapping charge is lower near the interface and higher as the charges approach the center of the LDPE, leading to a substantial accumulation of charges in the center of the sample as the applied electric field increase, and charge transport in steady state is dominated by the trapped charges.

Keywords: Space charge, LDPE, BCT, Field-Dependent Parameters.

ARTICLE INFORMATION

Author(s): Boukhari Hamed, Youcef Abdallah Baadj, and Fatiha ROGTI;

Received: 25/02/2025; **Accepted:** 06/06/2025; **Published:** 10/06/2025;

E- ISSN: 2347-470X;

Paper Id: IJEER 2502-02;

Citation: 10.37391/ijeer.130209

Webpage-link:

<https://ijeer.forexjournal.co.in/archive/volume-13/ijeer-130209.html>



Publisher's Note: FOREX Publication stays neutral with regard to jurisdictional claims in Published maps and institutional affiliations.

1. INTRODUCTION

Solid polymeric materials, especially Low-density polyethylene (LDPE), play a key role in electrical energy transportation due to their outstanding mechanical, thermal, and dielectric properties and low cost, They are widely used as insulating materials, particularly in high-voltage cable systems[1-10]. However, one of the major problems related to uses of LDPE especially under high-voltage direct-current (HVDC) applications, is the formation of space charge within the bulk of the insulating material[5, 11, 12]. The presence of space charge in insulating materials can distort the electric field distribution, potentially leading to insulation degradation and, ultimately and electrical breakdown [5, 13].

For this reason, HVDC cables can only perform better if we understand the mechanisms of charge transport and accumulation within solid polymeric dielectrics [11]. In fact, a complete understanding of electron and hole transport in polymers like low-density polyethylene (LDPE) and cross-linked polyethylene (XLPE) has not yet been achieved [5, 14]. Although this topic has been extensively researched for two decades, it remains unclear and lacks an unambiguous explanation[15].

Regarding experimental studies, several non-destructive measurement techniques have been developed to measure space charge distributions. These methods include the pulsed electro-acoustic (PEA) method [16], the thermal step (TSM) method [17], and the pressure wave propagation (PWP) method [18]. For example, using the PEA method, acoustic waves are generated from space charges under an applied electric field. These waves are captured by a piezoelectric sensor, converted into electrical signals, amplified, and then recorded. Digital processing is utilized to reconstruct the profile of the space charges[19].

Regarding numerical simulation studies, more microscopic approaches (Known also as mesoscopic models) have been developed over the past two decades [15, 17]. These approaches rely on bipolar charge transport (BCT) and incorporate charge generation, as well as transport processes involving trapping, detrapping and recombination. The majority of materials used are polyethylene-based [20].

Researchers are exploring numerical simulation methods to the space charge dynamics in polymer insulation, aiming to quantitatively describe charge transport and accumulation over a wide temperature range long durations, and complex structures[10, 16].

The first model of BCT in degassed XLPE was proposed by Alison in 1994 [21]. This model involves double injection and extraction of charge carriers at the electrodes without potential barriers, with charge transport occurring at a constant mobility and trapping in deep sites. Fukuma et al [22] proposed a bipolar model for XLPE under DC voltage, involving Schottky charge injection and hopping transport for both species. Charge extraction occurs via barriers, with recombination considered only between mobile species. Kaneko et al [9] present an asymmetric bipolar model for LDPE, based on similar assumptions to those of Alison and Hill. Charge generation occurs through Schottky injection, with conduction via hopping and no deep trapping. Charge recombination happens between holes and electrons, and charge extraction at the opposite electrode is continuous. LeRoy et al [23] presented a macroscopic bipolar model based on Alison's model, featuring Schottky injection and a thermally activated deep trap detrapping barrier. The simulated sample is LDPE with an initial charge density added to replicate experiments. The results are compared to experimental measurements of space charge, luminescence, and currents. Boufayed et al. [24] present a macroscopic bipolar model for cross-linked polyethylene (XLPE) based on Le Roy's model. It includes an exponential distribution for trapping and a maximum trap depth, replacing the single deep trap level. The model considers Schottky injection for both charge carriers and introduces mobility dependence on trap filling, with charge transport via hopping for a fraction of the charges, excluding recombination effects. Belgaroui et al [25] present a microscopic bipolar model based on Alison's model for low and high applied voltages. They introduce a new numerical method for solving the model

equations using the Finite Element Method (FEM) and high-order Runge-Kutta method. At high voltage, the model reveals the formation of charge packets (electrons and holes) for the first time.

In subsequent years, various bipolar models based on Alison and Le Roy's models were developed. Each model considered specific assumptions for charge generation or transport to adapt their models to the targeted application [20].

In recent modeling studies, charge transport parameters in polymeric insulators, such as charge carrier mobility, trapping probability, and recombination rates, are generally considered constant, without accounting for the electric field. Subsequently, several studies incorporated field-dependent mobility models such as hopping transport [9, 22] and the Poole-Frenkel effect to account for the influence of the electric field on charge carrier motion. After that, recombination rates were modified in some works as functions of field-dependent mobility (e.g., via Langevin-type models)[15], but other parameters in the models remained constant. In this work, we propose a new bipolar charge transport model in LDPE based on the Alison and Le Roy models, with Field-Dependent Parameters such as mobility, trapping, and recombination. The model includes hopping mobility affected by the electric field, and both the trapping probability and recombination rates are expressed as functions of mobility. Consequently, all processes vary dynamically with the applied electric field. This model presents a new step in the numerical simulation of charge behavior under high DC stress, offering a more realistic and accurate description of the physical phenomena in dielectric materials. The main physical features of several BCT models are presented in *table 1*.

Table 1. Characteristics of physical BCT models

Features	Alison et al [21]	Kaneko et al	LeRoy et al [23]	D. Min et al [26]	LeRoy et al [15]	Our Model
Trap Level	Single deep trap level	Two trap levels	Single deep trap level	Single deep trap level	Single deep trap level	Single deep trap level
Transport	Free carrier conduction	Hopping conduction	Free carrier conduction	Free carrier conduction	Hopping conduction	Hopping conduction
Field-Dependent Transport	Trapping coefficient	Coefficients for acceptor and intermediate levels Coefficients for acceptor and intermediate levels	Trapping coefficient and detrapping barrier	Coulomb trap model dependent on effective mobility and detrapping barrier	Trapping coefficient and detrapping barrier	Coulomb trap model with trapping probability dependent on field-dependent mobility and detrapping barrier.
Charge Injection	Injection through electrodes	Schottky injection	Schottky injection	Schottky injection	Schottky injection	Schottky injection
Charge Extraction	No extraction barrier	Extraction barrier	No extraction barrier	No extraction barrier	No extraction barrier	No extraction barrier
Recombination	Recombination coefficient	Recombination coefficient	Recombination coefficients	Langevin models dependent on mobility	Langevin models dependent on field-dependent mobility	Langevin models dependent on field-dependent mobility

We consider a sample of low-density polyethylene (LDPE) with a thickness of 100 μm , sandwiched between two electrodes (*i.e.*, anode and cathode). This one-dimensional, symmetric model is designed to describe the spatial and temporal evolution of space charge generated by the injection of charged particles (electrons and holes) at each electrode under DC electric field at room temperature. According to the Schottky law, charge injection and transport in shallow traps within the bulk of the sample exhibit field-dependent mobility, characterized by hopping mechanisms [11]. Each type of carrier is trapped at a single level of deep traps, with the trapping probability being dependent on mobility, following the Coulomb trap mode [20, 26]. The charge trapped can be detrapped using a thermally activated coefficient. Recombination of opposite sign charges by Langevin type with mobility dependent, parameters is also included in the model [15, 26, 27]. The bipolar charge transport model is schematically represented in figure 1.

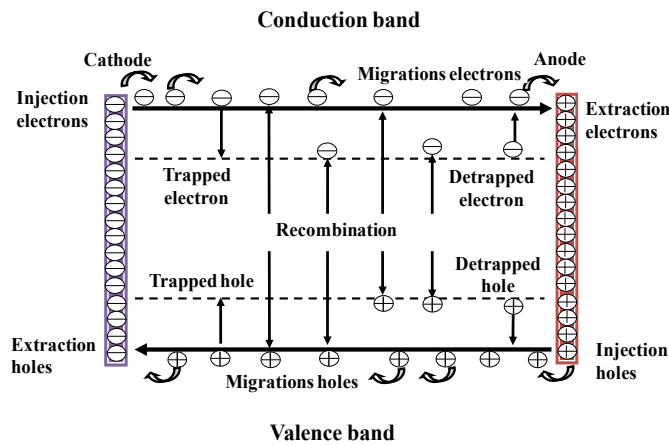


Figure 1. Schematic of bipolar charge model [11].

2. MATHEMATICAL MODEL DESCRIPTION

The BCT model assumes that there are four types of carriers within the insulating material: free electrons ($e\mu$), free holes ($h\mu$), trapped electrons (et), and trapped holes (ht). Theoretically, the behavior of charge carriers in solid dielectric materials is governed by three fundamental equations: Poisson's equation, the transport equation, and the continuity equation [28-32]. These equations describe the charge density, current density, and electric fields as functions of time and spatial position, neglecting diffusion. They are as follows:

$$\frac{\partial^2 \Phi(x,t)}{\partial x^2} = \frac{q_{nt}(x,t)}{\epsilon_r \epsilon_0} \quad (1)$$

$$\text{grad}(\Phi(x,t)) = -E(x,t) \quad (2)$$

$$\frac{\partial q_{(e,h)\mu}(x,t)}{\partial t} + \frac{\partial j_{(e,h)}(x,t)}{\partial x} = S \quad (3)$$

$$j_{(e,h)}(x,t) = \mu_{(e,h)}(x,t) q_{(e,h)\mu}(x,t) E(x,t) \quad (4)$$

All parameters of our model are classified in the table 2.

Table 2. Parameters of the model [14-25]

Parameters	Nomenclature	Unit
x	Spatial coordinate	[m]
t	Times	[s]
ϵ_r	Relative dielectric permittivity	
ϵ_0	Vacuum permittivity	[F/m]
d	Separation between trap sites	[m]
D	Dielectric thickness	[m]
ν	Attempt-to-escape frequency	[s ⁻¹]
K_b	Boltzmann constant	[J.K ⁻¹]
T	Temperature	[K]
S	Source terms	
N	Trap density	[C.m ⁻³]
A	Richardson constant	[A.m]
e	Elementary electronic charge	[C]
$w_{hp(e,h)}$	Hopping energy level of trap depth for electron and hole	[eV]
$w_{in(e,h)}$	Injection barrier heights for electrons and holes	[eV]
$w_{dt(e,h)}$	Detrapping barrier for electron and hole	[eV]
$N_{t(e,h)}$	Trap density of electrons and holes	[C.m ⁻³]
E	Electric field	[kV/mm]
$\Phi(x,t)$	Local potential	[kV]
$q_{(e,h)\mu}$	Mobile charge density of the electrons and holes	[C.m ⁻³]
$q_{(e,h)t}$	Trapped charge density of the electrons and holes	[C.m ⁻³]
$q_{nt}(x,t)$	Net charge density	[C.m ⁻³]
$\mu_{(e,h)}(x,t)$	Carrier mobility of electrons and holes	[m ² V ⁻¹ s ⁻¹]
$P_{t(e,h)}$	Trapping probability of electrons and holes	[s ⁻¹]
$P_{D(e,h)}$	Detrapping probability of electrons and holes	[s ⁻¹]
$R_{(et,h\mu)}$	Recombination rate of trapped electrons and trapped holes	[m ³ C ⁻¹ s ⁻¹]
$R_{(e\mu,ht)}$	Recombination rate of mobile electron and trapped holes	[m ³ C ⁻¹ s ⁻¹]
$R_{(et,ht)}$	Recombination rate of trapped electrons and mobile holes	[m ³ C ⁻¹ s ⁻¹]
$R_{(e\mu,h\mu)}$	Recombination rate of mobile electrons and mobile	[m ³ C ⁻¹ s ⁻¹]
Q_M	Quantity of mobile charges	[C.m ⁻²]
Q_A	Quantity of trapped charges	[C.m ⁻²]
$j_{(e,h)}$	Conduction current density of the electrons and holes	[A.m ⁻²]
$j_d(x,t)$	External current density	[A.m ⁻²]
$j_{ext}(x,t)$	Displacement current	[A.m ⁻²]

Charge transport of free carriers is described by a hopping mechanism, where carriers move from site to site by tunneling through a potential barrier, influenced by the electric field and temperature, as shown in the equation [15, 20]:

$$\mu_{(e,h)}(x, t) = \frac{2vd}{E(x,t)} \exp\left(-\frac{eW_{hp}(e,h)}{k_bT}\right) \sinh\left(\frac{eE(x,t)d}{2k_bT}\right) \quad (5)$$

The defined net charge density is as follows:

$$q_{nt}(x, t) = q_{h\mu}(x, t) + q_{ht}(x, t) - q_{e\mu}(x, t) - q_{et}(x, t) \quad (6)$$

Charge generation (electrons and holes) is assumed to be controlled by Schottky thermionic emission at the electrode-dielectric interface, where the fluxes are influenced by the local electric field and temperature, as shown in the equations [12, 33, 34]:

$$j_e(0, t) = AT^2 \exp\left(-\frac{eW_{in e}}{k_bT}\right) \exp\left(\frac{e}{k_bT} \sqrt{\frac{eE(0,t)}{4\pi\epsilon}}\right) \quad (7)$$

$$j_h(D, t) = AT^2 \exp\left(-\frac{eW_{in h}}{k_bT}\right) \exp\left(\frac{e}{k_bT} \sqrt{\frac{eE(D,t)}{4\pi\epsilon}}\right) \quad (8)$$

Where $j_e(0, t)$ and $j_h(D, t)$ represent the injection current densities at the cathode and anode, respectively.

$E(0, t)$ and $E(D, t)$ are the electric fields at the cathode and the anode, respectively. We assume the absence of extraction barriers, and the extraction current densities for electrons and holes from the cathode and anode electrodes, respectively, are described by [11, 23]:

$$j_e(D, t) = \mu_e(x, t) q_{e\mu}(D, t) E(D, t) \quad (9)$$

$$j_h(0, t) = \mu_h(x, t) q_{h\mu}(0, t) E(0, t) \quad (10)$$

Where $j_e(D, t)$ and $j_h(0, t)$ represent the flux of electrons and holes at the anode and cathode, respectively.

The trapping probability to deep trap centers for electrons and holes, being dependent on field-dependent mobility (Coulomb trap model), can be given by the following equation [20, 26, 35, 36]:

$$P_{t(e,h)} = \mu_{(e,h)}(x, t) e N_{t(e,h)} \quad (11)$$

Trapped charges may be released after being held in trap centers for a certain duration. The detrapping probability for electrons and holes is expressed as [23, 36, 37]:

$$P_{D(e,h)} = v. \exp\left(\frac{eW_{dt}(e,h)}{k_bT}\right) \quad (12)$$

The mobility of mobile electron carriers determines the recombination rate between mobile electrons and trapped holes. Similarly, the recombination rates between mobile holes and trapped electrons are determined by the mobility of mobile hole carriers. This model ignores recombination between trapped electrons and trapped holes [15, 26]:

$$R_{(e\mu, h\mu)} = q_{e\mu}(x, t) q_{h\mu}(x, t) (\mu_e(x, t) + \mu_h(x, t)) / \epsilon_r \epsilon_0 \quad (13)$$

$$R_{(e\mu, ht)} = q_{e\mu}(x, t) q_{ht}(x, t) \mu_e(x, t) / \epsilon_r \epsilon_0 \quad (14)$$

$$R_{(et, h\mu)} = q_{et}(x, t) q_{h\mu}(x, t) \mu_h(x, t) / \epsilon_r \epsilon_0 \quad (15)$$

$$R_{(et, ht)} = 0 \quad (16)$$

Source terms are defined for each charge type, mobile or trapped, as follows [11, 38, 39]:

$$S_{e\mu} = -R_{(e\mu, h\mu)} q_{e\mu}(x, t) q_{h\mu}(x, t) - R_{(e\mu, ht)} q_{e\mu}(x, t) q_{ht}(x, t) - P_{t(e)} q_{e\mu}(x, t) \left(1 - \frac{q_{et}(x, t)}{N_e}\right) + P_{D(e)} q_{et}(x, t) \quad (17)$$

$$S_{et} = -R_{(et, ht)} q_{et}(x, t) q_{ht}(x, t) - R_{(et, h\mu)} q_{et}(x, t) q_{h\mu}(x, t) + P_{t(e)} q_{e\mu}(x, t) \left(1 - \frac{q_{et}(x, t)}{N_e}\right) - P_{D(e)} q_{et}(x, t) \quad (18)$$

$$S_{h\mu} = -R_{(e\mu, h\mu)} q_{h\mu}(x, t) q_{e\mu}(x, t) - R_{(et, h\mu)} q_{h\mu}(x, t) q_{et}(x, t) - P_{t(h)} q_{h\mu}(x, t) \left(1 - \frac{q_{ht}(x, t)}{N_h}\right) + P_{D(h)} q_{ht}(x, t) \quad (19)$$

$$S_{ht} = -R_{(et, h\mu)} q_{et}(x, t) q_{ht}(x, t) - R_{(e\mu, ht)} q_{ht}(x, t) q_{e\mu}(x, t) + B_h q_{h\mu}(x, t) \left(1 - \frac{q_{ht}(x, t)}{N_h}\right) - P_{D(h)} q_{ht}(x, t) \quad (20)$$

The quantity of mobile Q_M and accumulated charges Q_A respectively calculated as [26, 35, 40]:

$$Q_M = \int_0^D q_{(e,h)\mu}(x, t) dx \quad (21)$$

$$Q_A = \int_0^D q_{(e,h)t}(x, t) dx \quad (22)$$

The expression for the local current density associated with the conduction of mobile electrons and holes is expressed as follows [11, 25]:

$$j_{(e,h)}(x, t) = \left(q_{e\mu}(x, t) \mu_e(x, t) + q_{h\mu}(x, t) \mu_h(x, t) \right) E(x, t) \quad (23)$$

The expression for the displacement current density is [29]:

$$j_d(x, t) = \epsilon \frac{\partial E(x, t)}{\partial t} \quad (24)$$

The density of the external current is represented by [31]:

$$j_{ext}(x, t) = \int_0^D [j_{(e,h)}(x, t) + j_d(x, t)] dx \quad (25)$$

The selection of numerical models in this work based on specific physical considerations and constraints. The Poisson, continuity, and transport equations are coupled by the electric field and charge density, necessitating the application of

specific models. To solve this model, finite element method was used to solve Poisson equation (Eq: 01) to determine the electric field distribution[25], which is applicable to complex configurations such as polyethylene electrical cables.

The continuity equation can be solved in two steps using a splitting method (Eq:03). First, the equation is solved without the source term, such that [39, 41, 42]:

$$\frac{\partial q_{(e,h)\mu}(x,t)}{\partial t} + \frac{\partial j_{(e,h)}(x,t)}{\partial x} = 0 \quad (26)$$

Secondly, the continuity equation, including source terms, is solved using the high-precision Runge–Kutta method to accurately calculate the densities of both mobile and trapped electrons and holes(Eq: 18-20), such that [25, 43]:

$$\frac{\partial q_{(e,h)\mu}(x,t)}{\partial t} = S \quad (27)$$

The complete flow of the numerical algorithm is illustrated in figure 2 .Through the numerical solution of the physical model, the temporal and spatial distribution of net charge density, electric field, average mobile and trapped density, trapping charge distribution, and external current density are obtained and studied in this work.

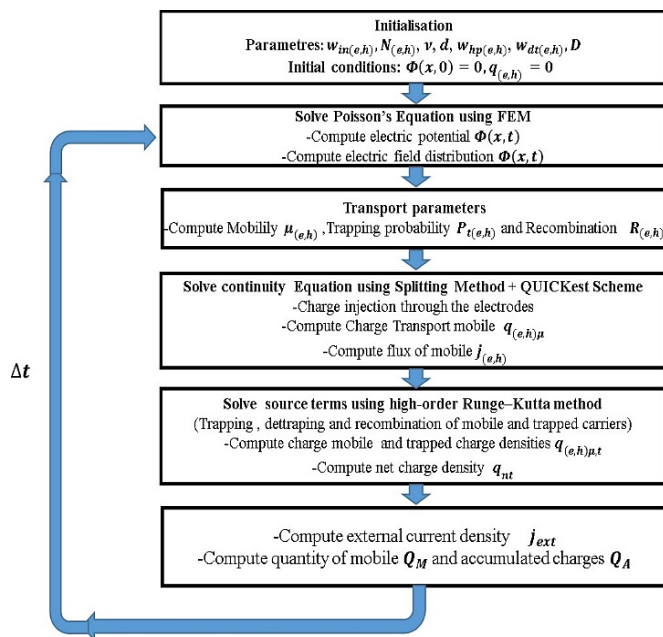


Figure 2. Numerical resolution flowchart for the BCT model

3. RESULT AND DISCUSSION

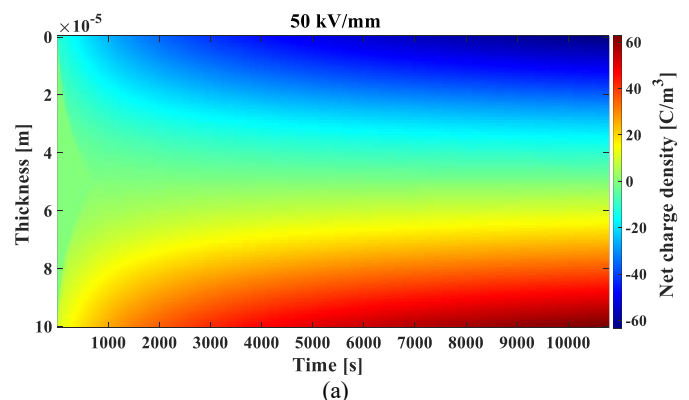
In this section, the numerical results of our models will be presented. LDPE film with a thickness of 100 μm was used in the simulation. The film was discretized into 100 non-uniform elements. Simulation parameters are selected based on parameter ranges estimated from experimental conditions and several previous works on BCT simulation in LDPE. A symmetrical value for parameters such as injection barrier

height, trap densities, detrapping barrier, and hopping energy level, used in the BCT simulations, is regrouped in table 3. Voltages of 5, 10, and 12 kV, corresponding to electric fields of 50, 100, and 120 kV/mm, respectively, were applied during 3 hours of simulation at room temperature (25 °C).

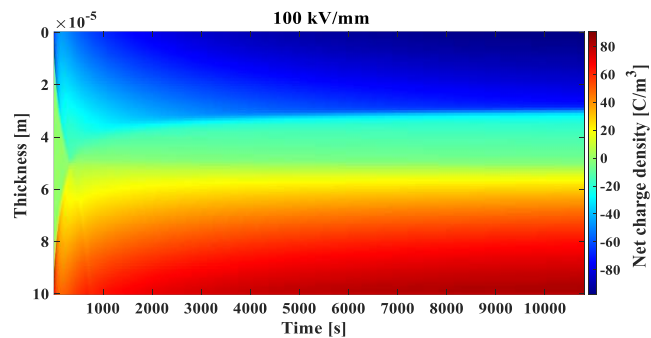
Table 3. Parameters values of the model

Injection barrier	$w_{in(e,h)} = 1.2 \text{ eV}$ [11]
Trap density	$N_{(e,h)} = 6.25 \times 10^{20} \text{ C.m}^{-3}$ [15]
Attempt-to-escape frequency	$\nu = 4 \times 10^{13} \text{ s}^{-1}$ [24]
Separation between trap sites	$d = 10^{-9} \text{ m}$ [24]
Trap depth	$w_{hp(e,h)} = 0.62 \text{ eV}$ [15]
Detrapping barrier	$w_{dt(e,h)} = 0.8 \text{ eV}$ [11]
Dielectric thickness	$D = 10^{-4} \text{ m}$ [11]

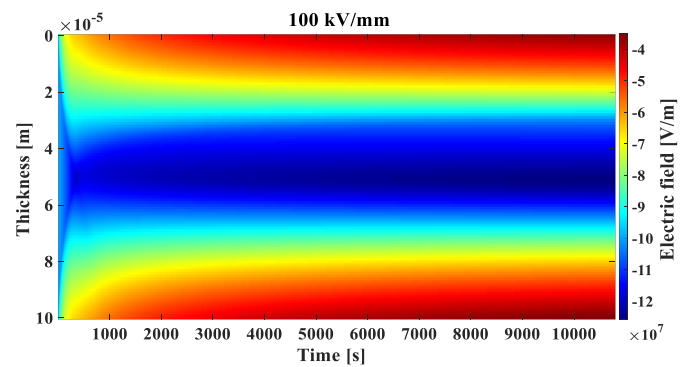
The results of net charge density as a function of space and time under different electric field applications of 50, 100, and 120 kV/mm are presented in figures 3a, 3b, and 3c, respectively. In figure 3a, after the application of the electric field, both negative and positive charge carriers are injected near the cathode and anode electrodes, with electrons transported toward the anode and holes moving in the opposite direction. During their transport, positive and negative charges trapped and meet in the center of the sample at 600 s, forming alternating regions known as heterocharge zones, these zones initiate the recombination process. Subsequently, a relatively uniform distribution of charges is observed over time. In figure 3b (at 100 kV/mm), charge injection and transport are more pronounced, resulting in steeper gradients near the electrodes and a faster spread of charges toward the center (at 530 s for heterocharges zones). This leads to higher net charge densities and quicker stabilization compared to the 50 kV/mm case. The same behavior is observed in figure 3c (at 120 kV/mm), with more charge injection and an even faster transport speed of positive and negative charges into the bulk of the sample (heterocharges zones at 510 s) compared to the 50 and 100 kV/mm case.



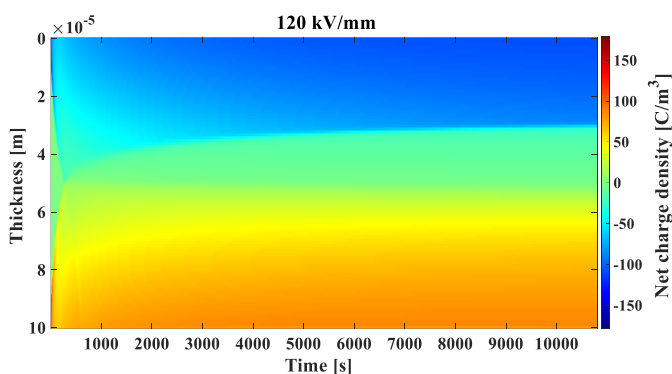
(a)



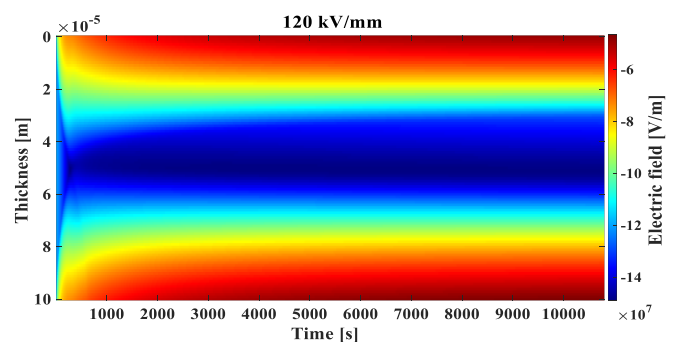
(a)



(a)



(b)



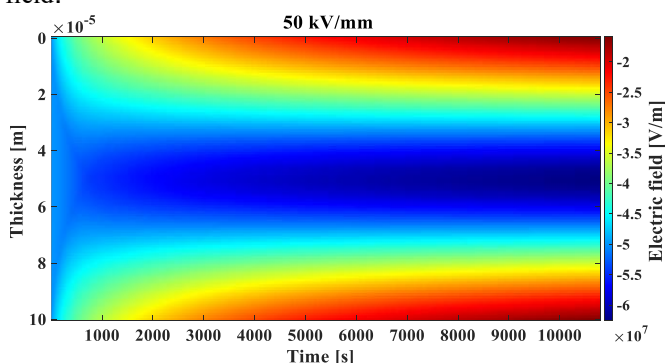
(b)

Figure 3. Net charge density as a function of time and space under DC electric field applied: (a) 50 kV/mm, (b) 100 kV/mm, (c) 120 kV/mm

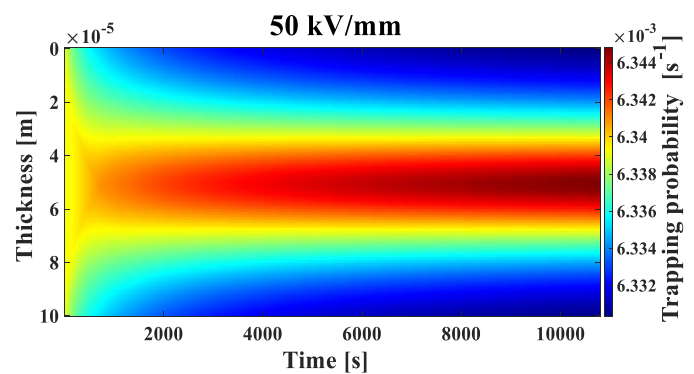
Figure 4. Electric field distribution as a function of time and space, under DC electric field applied: (a) 50 kV/mm, (b) 100 kV/mm, (c) 120 kV/mm

Space-charge accumulation in the LDPE leads to significant distortion of the internal electric field distribution. *Figure 4a, b, and c* present the electric field distribution in LDPE as a function of space and time under 50, 100, and 120 kV/mm, respectively. Initially, the electric field distribution is uniform across the sample thickness. However, as space charges accumulate over time, a clear distortion emerges, the field near the cathode and anode interfaces decreases markedly, while the field intensity in the middle of sample increases. This behavior becomes more pronounced with increasing applied electric field. Specifically, for applied fields of 50, 100, and 120 kV/mm, the peak electric field in the mid-plane of the sample reaches about 59, 119, and 139 kV/mm, corresponding to distortion ratios of 18%, 19%, and 20%, respectively at around 3 h. These results show that more pronounced and faster the field distortion, results from increased space-charge injection, transport, and trapping processes in the stronger the applied field.

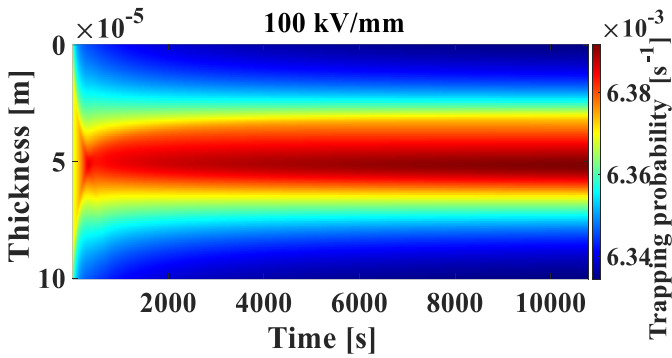
Carrier mobility in this model is field-dependent, trapping probability and recombination rates are functions of mobility. *Figures 5a, 5b, and 5c* illustrate the spatiotemporal distribution of trapping probability in LDPE under applied fields of 50, 100, and 120 kV/mm, respectively. The results indicate that the trapping probability distribution exhibits behavior similar to the electric field distribution in the sample, with increasing trapped charge probability in the bulk of the sample relative to the interfaces. This explains the significant distortion of the electric field observed in the bulk of the sample, as shown in *Figure 4*, which is due to the substantial trapped charges compared to those at the sample's interface. The maximum trapping in the middle of the sample is approximately 6.344×10^{-3} , 6.38×10^{-3} , and $6.41 \times 10^{-3} \text{ s}^{-1}$ at 3 hours for applied electric fields of 50, 100, and 120 kV/mm, respectively.



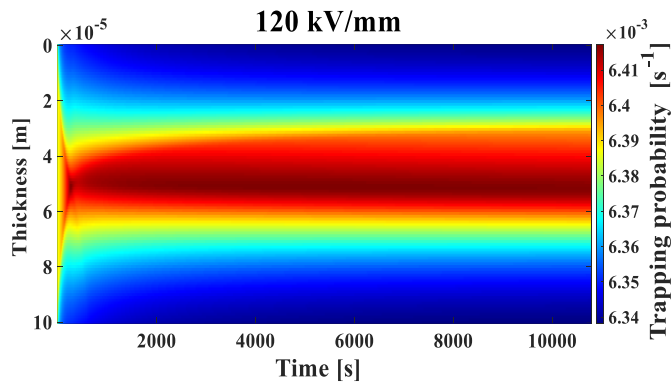
(c)



(c)



(b)

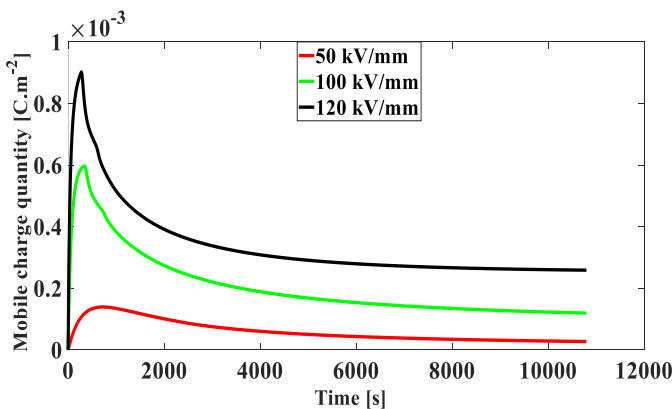


(c)

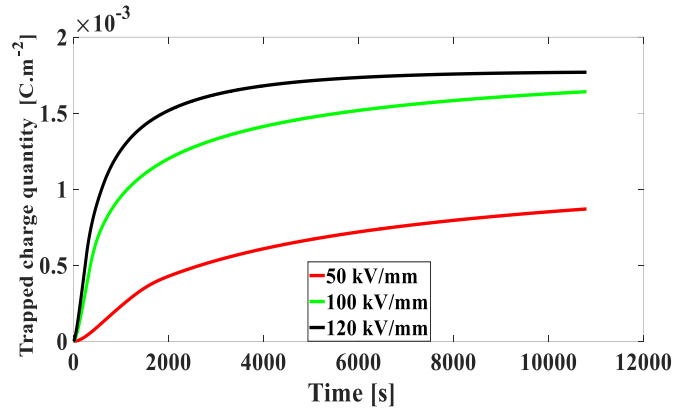
Figure 5. Trapping probability distribution as a function of time and space, under DC electric field applied: (a) 50 kV/mm, (b) 100 kV/mm, (c) 120 kV/mm

Figures 6a and 6b present the quantities of mobile and trapped charges in LDPE as a function of time under 50, 100, and 120 kV/mm. We observe that the quantity of mobile charge initially increases rapidly until it reaches a maximum. The maximum quantity of mobile charge density is approximately 6.344×10^{-3} , 6.38×10^{-3} , and 6.41×10^{-3} at 600, 530 and 510 s for applied electric fields of 50, 100, and 120 kV/mm, respectively.

This behavior is more pronounced as the applied electric field increases, as shown for 100 kV/mm and 120 kV/mm.



(a)



(b)

Figures 6. Quantities of mobile and trapped charges in LDPE as a function of time under 50, 100, and 120 kV/mm. a- Quantities of mobile charges. b-Quantities of trapped charges

At this point, the mobile negative and positive charges reach the middle of the sample, and the quantity of mobile charge decreases due to recombination and trapping, which are higher in this region. The quantity of mobile charges continues to decrease until it reaches a steady state. In contrast, the quantity of trapped charges continues to increase until it reaches a steady state. As the applied electric field increases, the quantity of trapped charges also increases, and the steady-state condition is reached more quickly, as illustrated in the figure 6b. From these results, we can conclude that as the electric field increases, most of the net charge density consists of trapped charges in the steady state.

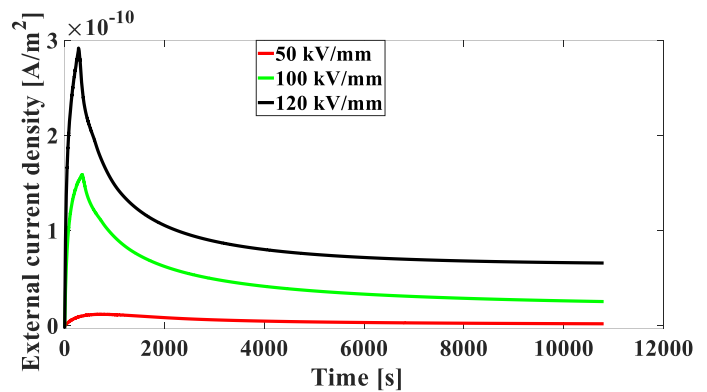


Figure 7. External current density in LDPE as a function of time under 50, 100, and 120 kV/mm

Figures 7 present the external current density in LDPE as a function of time under 50, 100, and 120 kV/mm. As shown in equation 10, the external current is always proportional to the mobile charge density. Then, when the electric field is applied, the current increases rapidly until it reaches its maximum value (1.344×10^{-11} , 1.38×10^{-10} , and $2.91 \times 10^{-10} \text{ A.m}^{-2}$ at 600, 530 and 510 s for applied electric fields of 50, 100, and 120 kV/mm, respectively). When the bipolar charges arrive to the center of the sample, the current decreases with time and achieves a steady state.

5. CONCLUSION

In this paper, BCT model used to studies dynamic of space charge in LDPE under DC electrical stress, such as injection, migration, trapping, detrapping and recombination. Based on the results obtained, we can conclude that the trapping charge probability as a function of the electric field in LDPE has a significant impact on the charge transport behavior in the sample compared to other parameters. Unlike all previous BCT simulation works in LDPE, which assume the trapping charge probability to be constant throughout the sample, our model considers that the trapping charge probability depends on the electric field distribution in the sample. It is lower near the interface and higher as the charges approach the center of the LDPE, leading to a substantial accumulation of charges in the center of the sample as the applied electric field increases. Meanwhile, the mobile charges decrease over time until reaching a steady state, where it becomes clear that the net charge density is dominated by the trapped charges.

ACKNOWLEDGMENTS

We gratefully acknowledge the Materials, Energy Systems Technology and Environment Laboratory at University of Ghardaia, Algeria for their essential support and the use of their facilities, which were instrumental in the successful completion of this research.

REFERENCES

- [1] V. Zakrevskii, N. Sudar, A. Zaopo, and Y. A. Dubitsky, "Mechanism of electrical degradation and breakdown of insulating polymers," *Journal of applied physics*, vol. 93, pp. 2135-2139, 2003.
- [2] G. Mazzanti, "Issues and challenges for HVDC extruded cable systems," *Energies*, vol. 14, p. 4504, 2021.
- [3] J. Wu, L. Lan, Z. Li, and Y. Yin, "Simulation of space charge behavior in LDPE with a modified of bipolar charge transport model," in *Proceedings of 2014 International Symposium on Electrical Insulating Materials*, 2014, pp. 65-68.
- [4] Y. Zhan, G. Chen, and M. Hao, "Space charge modelling in HVDC extruded cable insulation," *IEEE Transactions on Dielectrics and Electrical Insulation*, vol. 26, pp. 43-50, 2019.
- [5] F. Rogti, "Effect of temperature on formation and stability of shallow trap at a dielectric interface of the multilayer," *Journal of Electronic Materials*, vol. 44, pp. 4655-4662, 2015.
- [6] L. Dissado, G. Mazzanti, and G. Montanari, "The role of trapped space charges in the electrical aging of insulating materials," *IEEE Transactions on Dielectrics and Electrical Insulation*, vol. 4, pp. 496-506, 1997.
- [7] C. Thomas, G. Teyssedre, and C. Laurent, "Space charge measurements in low-density polyethylene under AC stress by the pulsed electro-acoustic method," in *2008 Annual Report Conference on Electrical Insulation and Dielectric Phenomena*, 2008, pp. 325-328.
- [8] G. Montanari, C. Laurent, G. Teyssedre, A. Campus, and U. Nilsson, "From LDPE to XLPE: investigating the change of electrical properties. Part I. space charge, conduction and lifetime," *IEEE Transactions on Dielectrics and Electrical Insulation*, vol. 12, pp. 438-446, 2005.
- [9] K. Kaneko, T. Mizutani, and Y. Suzuoki, "Computer simulation on formation of space charge packets in XLPE films," *IEEE Transactions on Dielectrics and Electrical Insulation*, vol. 6, pp. 152-158, 1999.
- [10] G. Chen, M. Hao, Z. Xu, A. Vaughan, J. Cao, and H. Wang, "Review of high voltage direct current cables," *CSEE Journal of Power and Energy Systems*, vol. 1, pp. 9-21, 2015.
- [11] H. Boukhari and F. Rogti, "Simulation of space charge dynamic in polyethylene under DC continuous electrical stress," *Journal of Electronic Materials*, vol. 45, pp. 5334-5340, 2016.
- [12] P. Liu, X. Pang, Z. Xie, T. Xu, S. Shi, P. Wu, H. Li, and Z. Peng, "Space charge characteristics in epoxy/nano-MgO composites: Experiment and two-dimensional model simulation," *Journal of applied physics*, vol. 132, 2022.
- [13] J. Xia, Y. Zhang, F. Zheng, Z. An, and Q. Lei, "Numerical analysis of packetlike charge behavior in low-density polyethylene by a Gunn effectlike model," *Journal of applied physics*, vol. 109, 2011.
- [14] F. Tian, Q. Lei, X. Wang, and Y. Wang, "Effect of deep trapping states on space charge suppression in polyethylene/ZnO nanocomposite," *Applied Physics Letters*, vol. 99, 2011.
- [15] S. Le Roy and M. Hoang, "A bipolar charge transport model to simulate the impact of nanometric scale processes on the space charge behaviour in polyethylene," *Journal of Physics D: Applied Physics*, vol. 55, p. 465303, 2022.
- [16] G. Rizzo, P. Romano, A. Imburgia, and G. Ala, "Review of the PEA method for space charge measurements on HVDC cables and mini-cables," *Energies*, vol. 12, p. 3512, 2019.
- [17] P. He, Y. Liu, B. Zhang, and J. He, "Determination of Parameters for Space Charge Simulation Based on Bipolar Charge Transport Model under a Divergent Electric Field," *IEEE Transactions on Dielectrics and Electrical Insulation*, 2024.
- [18] R. Liu, L. Johansson, M. Lundmark, and G. Wahlstrom, "Pressure wave propagation technique to investigate water treeing degradation in polymers," in *Proceedings of 1994 IEEE International Symposium on Electrical Insulation*, 1994, pp. 383-386.
- [19] E. Doedens, E. M. Jarvid, R. Guffond, and Y. V. Serdyuk, "Space charge accumulation at material interfaces in HVDC cable insulation Part II— Simulations of charge transport," *Energies*, vol. 13, p. 1750, 2020.
- [20] X. Zhu, J. Wu, Y. Wang, and Y. Yin, "Review of Numerical Simulation of Charge Transport in Polymer Insulation Under a High Electric Field and Its Application," *IEEE Electrical Insulation Magazine*, vol. 40, pp. 14-32, 2024.
- [21] J. Alison and R. Hill, "A model for bipolar charge transport, trapping and recombination in degassed crosslinked polyethene," *Journal of Physics D: Applied Physics*, vol. 27, p. 1291, 1994.
- [22] M. Fukuma, M. Nagao, and M. Kosaki, "Computer analysis on transient space charge distribution in polymer," in *Proceedings of 1994 4th International Conference on Properties and Applications of Dielectric Materials (ICPADM)*, 1994, pp. 24-27.
- [23] S. Le Roy, P. Segur, G. Teyssedre, and C. Laurent, "Description of bipolar charge transport in polyethylene using a fluid model with a constant mobility: model prediction," *Journal of Physics D: Applied Physics*, vol. 37, p. 298, 2003.
- [24] F. Boufayed, G. Teyssedre, C. Laurent, S. Le Roy, L. A. Dissado, P. Ségur, and G. Montanari, "Models of bipolar charge transport in polyethylene," *Journal of applied physics*, vol. 100, 2006.
- [25] E. Belgaroui, I. Boukhris, A. Kallel, G. Teyssedre, and C. Laurent, "A new numerical model applied to bipolar charge transport, trapping and recombination under low and high dc voltages," *Journal of Physics D: Applied Physics*, vol. 40, p. 6760, 2007.
- [26] D. Min, W. Wang, and S. Li, "Numerical analysis of space charge accumulation and conduction properties in LDPE nanodielectrics," *IEEE*

- Transactions on Dielectrics and Electrical Insulation*, vol. 22, pp. 1483-1491, 2015.
- [27] Y. Liu, K. Zojer, B. Lassen, J. Kjelstrup-Hansen, H.-G. n. Rubahn, and M. Madsen, "Role of the charge-transfer state in reduced langevin recombination in organic solar cells: a theoretical study," *The Journal of Physical Chemistry C*, vol. 119, pp. 26588-26597, 2015.
- [28] F. Boughariou, S. Chouikhi, A. Kallel, and E. Belgaroui, "Bipolar model for electrical breakdown in polyethylene materials under dc high electrical fields," *Journal of Electrostatics*, vol. 76, pp. 54-61, 2015.
- [29] I. Boukhris, E. Belgaroui, and A. Kallel, "Post breakdown and lifetime of low density polyethylene film under generated transient charge packets," *The European Physical Journal-Applied Physics*, vol. 60, p. 10203, 2012.
- [30] A. Gargouri, I. Boukhris, E. Belgaroui, and A. Kallel, "Packet charge dynamic in thin polyethylene under high dc voltage," *Journal of Theoretical and Applied Physics*, vol. 7, pp. 1-7, 2013.
- [31] S. Chouikhi, I. Boukhris, E. Belgaroui, and A. Kallel, "Space charge packets in polyethylene nano-scales under dc applied voltages," *Journal of Electrostatics*, vol. 71, pp. 14-20, 2013.
- [32] S. Le Roy, G. Teyssedre, C. Laurent, G. Montanari, and F. Palmieri, "Description of charge transport in polyethylene using a fluid model with a constant mobility: fitting model and experiments," *Journal of Physics D: Applied Physics*, vol. 39, p. 1427, 2006.
- [33] J. Li, X. Qi, B. Du, H. Liang, M. Xiao, H. Sun, Z. Li, T. Han, M. Xiao, and Y. Li, "Simulation of interface charge behaviors in HVDC cable accessory based on bipolar carrier transportation model," in *2018 IEEE 2nd International Conference on Dielectrics (ICD)*, 2018, pp. 1-4.
- [34] Z. Xing, C. Zhang, M. Han, Z. Gao, Q. Wu, and D. Min, "A comparison of electrical breakdown models for polyethylene nanocomposites," *Applied Sciences*, vol. 12, p. 6157, 2022.
- [35] T.-c. Zhou, G. Chen, R.-j. Liao, and Z. Xu, "Charge trapping and detrapping in polymeric materials: Trapping parameters," *Journal of applied physics*, vol. 110, 2011.
- [36] G. Chen and Z. Xu, "Charge trapping and detrapping in polymeric materials," *Journal of applied physics*, vol. 106, 2009.
- [37] I. Boukhris, E. Belgaroui, and A. Kallel, "Physical and Numerical Modelling for Bipolar Charge Transport in Disorder Polyethylene Under High DC Voltage," *International Journal on Electrical Engineering and Informatics*, vol. 2, p. 313, 2010.
- [38] K. Hallak, F. Baudoin, V. Griseri, F. Bugarin, and S. Segonds, "A new approach for optimizing a bipolar charge transport model for dielectric materials: Theoretical framework," *IEEE Transactions on Dielectrics and Electrical Insulation*, vol. 28, pp. 872-879, 2021.
- [39] F. Ragazzi, A. Popoli, and A. Cristofolini, "An Efficient Numerical Technique for the Simulation of Charge Transport in Polymeric Dielectrics," *IEEE Access*, 2024.
- [40] C. Zhou and G. Chen, "Space charge behaviours in polyethylene under combined AC and DC electric fields," in *2014 IEEE Conference on Electrical Insulation and Dielectric Phenomena (CEIDP)*, 2014, pp. 848-851.
- [41] S. Le Roy, "Numerical methods in the simulation of charge transport in solid dielectrics," *IEEE Transactions on Dielectrics and Electrical Insulation*, vol. 13, pp. 239-246, 2006.
- [42] B. Leonard, "Universal limiter for transient interpolation modeling of the advective transport equations: the ULTIMATE conservative difference scheme," 1988.
- [43] J. Tian, J. Zou, Y. Wang, J. Liu, J. Yuan, and Y. Zhou, "Simulation of bipolar charge transport with trapping and recombination in polymeric insulators using Runge-Kutta discontinuous Galerkin method," *Journal of Physics D: Applied Physics*, vol. 41, p. 195416, 2008.



© 2025 by the Boukhari Hamed, Youcef Abdallah Baadj, and Fatiha ROGTL. Submitted for possible open access publication under the terms and conditions of the Creative Commons Attribution (CC BY) license (<http://creativecommons.org/licenses/by/4.0/>).